Efficient electricity storage with a battolyser, an integrated Ni-Fe battery and electrolyser

Mulder, F. M.; Weninger, B. M.H.; Middelkoop, J.; Ooms, F. G.B.; Schreuders, H.

Important note
To cite this publication, please use the final published version (if applicable).
Please check the document version above.

ELECTRONIC SUPPLEMENTARY INFORMATION

Efficient electricity storage with the battolyser, an integrated Ni-Fe battery and electrolyser

F.M. Mulder,[a] B.M.H. Weninger,[a] J. Middelkoop,[a] F.G.B. Ooms[b] and H. Schreuders[a]

[a.] *Materials for Energy Conversion and Storage (MECS), Department of Chemical Engineering, Delft University of Technology, Van der Maasweg 9, 2629HZ Delft, The Netherlands.*

[b.] *Fundamental Aspects of Materials and Energy (FAME), Department of Radiation Science and Technology, Delft University of Technology, Mekelweg 15, 2629 JB Delft, The Netherlands.*

Supplementary Figures 1-6:

Supplementary Tables 1-3:

References

Supplementary Figure 1, Battolyser layout.

(Left) Picture of assembled battolyser with in this case two negative and two positive electrodes.

(Right) Exploded view indicating the positions of the four electrodes, four electrical wire connections, gas exhausts and electrolyte inlets, as well as three gas separation diaphragms.
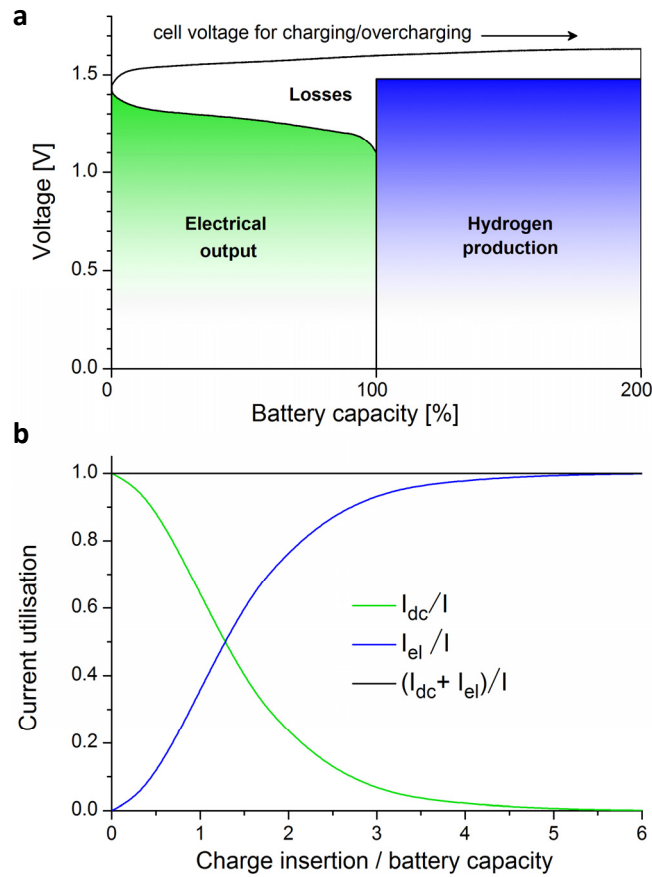
Supplementary Figure 2, Energy efficiency and charge utilisation.

(a) The total electrical energy input is given by integrating the experimental cell voltage during the charge and overcharge. The electrical energy output is given by the green area, while the hydrogen output is represented by the blue area corresponding with the thermal neutral potential times the inserted charge. The white area corresponds to the energy losses. The overall charge that is inserted comes back as either discharge of the battery or as hydrogen; as described the faradaic efficiency is 100% within the experimental accuracy of ±0.5%. Total and partial energy efficiencies ($\eta_{battery}$, $\eta_{electrolyser}$) are given by dividing the relevant area's by the total inserted energy (green, blue plus white area).

(b) The utilisation of the inserted current I as represented by I_{dc}/I and I_{el}/I from equation (11) and (12) as a function of the total inserted charge. Initially all charge is used for charging the battery, but the charge for electrolysis increases from the beginning. When the inserted charge equals the nominal battery capacity (value 1 on the x-axis) the Ni-Fe electrodes already produce significant hydrogen and oxygen, which is a reason why Ni-Fe batteries historically reached low energy efficiencies of ~60-70%[1,2]. In the battolyser charging can continue to many times this nominal capacity and the actual saturation in our experiments reaches C_{cap} = 14.5Ah or 1.45 times the nominal capacity.
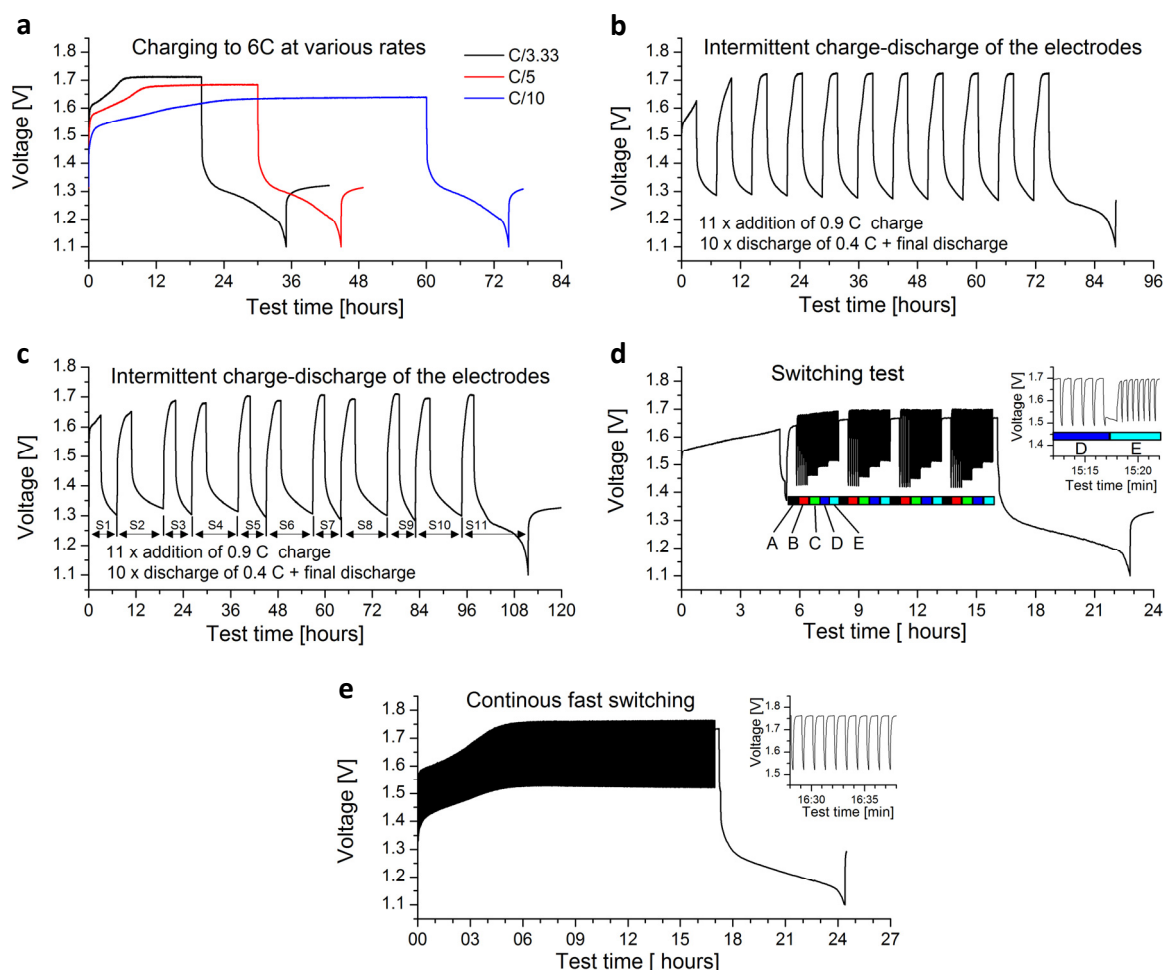
Supplementary Figure 3, Charge and switching capabilities (exemplary test cycles).

(a) Charging to 6 C (60Ah) at various charge rates; discharge at C/10 rate (this is a current of 1A, see Experimental section)

(b) Current handling capabilities of the charged electrodes, showing charge, electrolysis and intermediate discharge capabilities, while still being able to fully discharge at the end of the cycle. Partial charge insertion of 0.9C is followed by discharge of 0.4C; 0.4C of the 0.9C is used each time to charge the battery and the remaining 0.5C part for electrolysis. Charge rate C/3.33 (or 3A), discharge rate C/10 (or 1A).

(c) Cycle with one of the highest aggregated current insertion (nr 113 in Fig. 4 and Supplementary Fig. 4).

(d) Switching test at charged electrodes: first 5 hour charge at C/3.33 rate then switching in sequences A to E. A: 30 min charging at constant rate C/3.33; B: 5 cycles 5 min charge followed by 1 min discharge; C: 2.5 min charge followed by 30 sec discharge; D: 50 sec charge followed by 10 sec discharge; E: 25 sec charge followed by 5 sec discharge; for B-E: charge rate C/2.5 and discharge rate C/5, average rate C/3.33; one minute rest between programs A-E. Note that for higher switching rate the difference in potential between charge and discharge decreases, leading to increased electrical efficiency.

(e) Continuous fast switching test, 1000 cycles of 50 sec charge insertion (C/2.5) and 10 sec of charge withdrawal (C/5) completed by a final discharge.
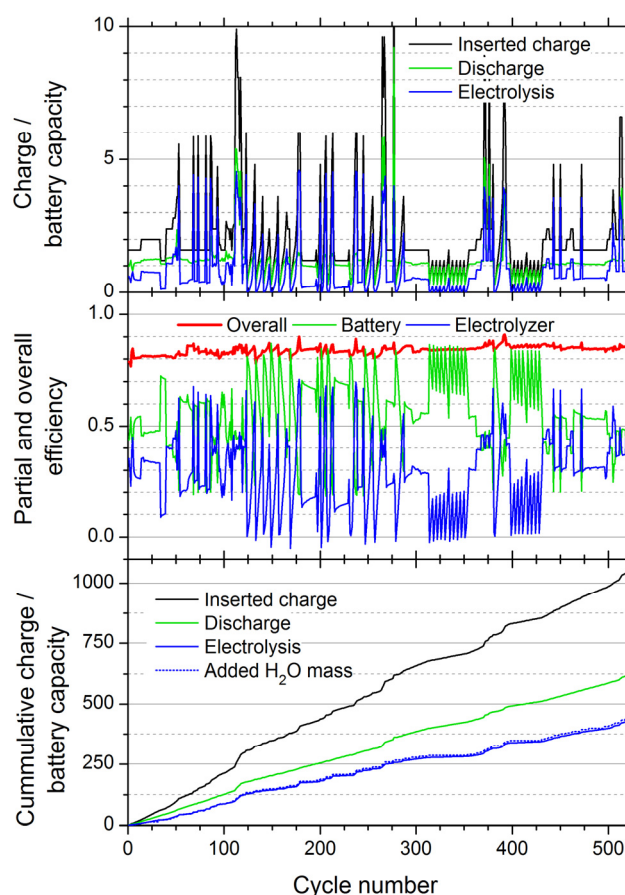
Supplementary Figure 4, Long term cycling and efficiencies.

This is an extension of Fig. 4b, where 4b is now in the lower panel for convenience.

(Top) Detail information on the inserted charge for a large number of cycles of a battolyser cell. A cycle is counted from full discharge to full discharge with various full or partial (over/dis)charge programs in between (so when there are many partial discharges and recharges before a final full discharge the aggregated discharge in that cycle can be much larger than the nominal capacity. See also Supplementary Tables 1-3). The inserted charge amounts vary strongly, from a fraction up to 10 times the nominal battery capacity insertion, and on average about two times the nominal battery capacity.

(Middle) Overall energy efficiency as sum of partial battery plus hydrogen gas efficiency (see Experimental Section). Depending on charge insertion amounts the H_2 production is much higher or lower than the battery charge. Consistently the overall cycle energy efficiency adds up to above 80 to 91%, with the highest battery (electrolysis) contribution to the efficiency at low (high) charge insertion. Sometimes the battery appears not fully discharged (for kinetic reasons) and then additional discharge capacity can be observed in subsequent cycles, leading to apparent over capacity and efficiency for the battery and under capacity and efficiency for electrolysis. These effects cancel each other in the total capacity and efficiency.

(Bottom, the same as Fig. 4b, shown here for convenience), Cumulative inserted charge and breakdown in battery charge and electrolysis, and the cumulative H_2O mass to replenish the electrolyte expressed with respect to the battery capacity.
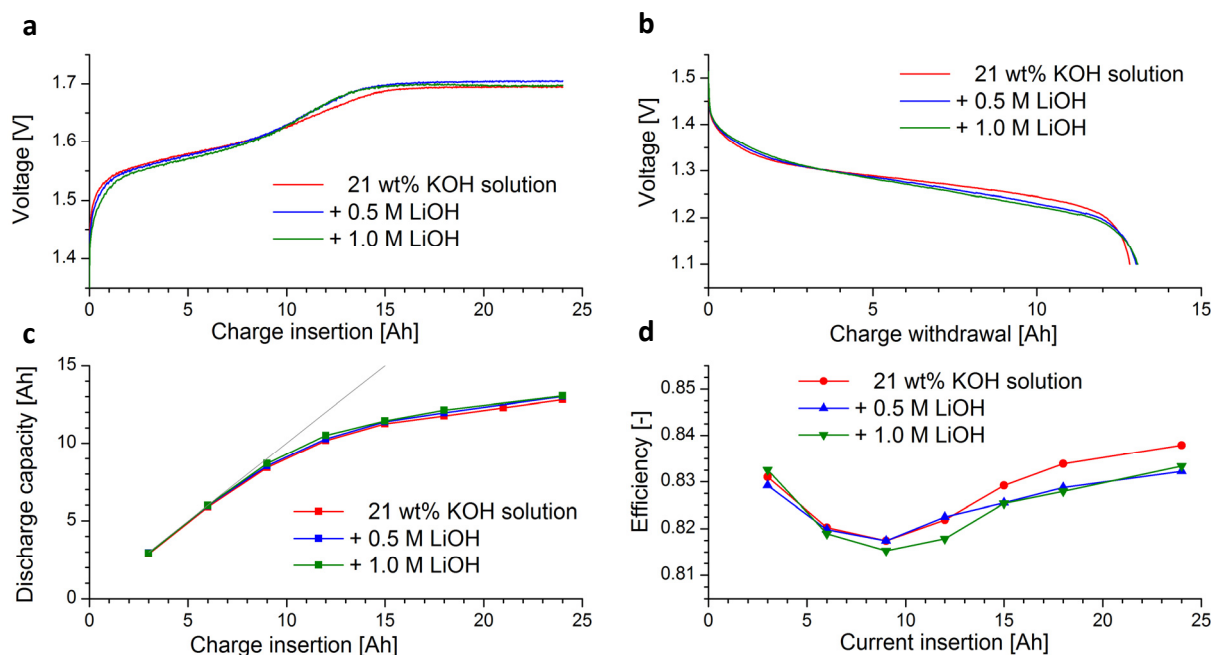
Supplementary Figure 5, Influence of LiOH addition of 21 wt% KOH electrolyte.

(a) Characteristic Charge curve using pure 21wt.% KOH electrolyte, and with the addition of 0.5 or 1.0 M/L LiOH. There is not much difference on the potentials i.e. the efficiencies, which makes that a small LiOH addition as described in [1, 3] for the battery functionality can be used.

(b) Characteristic discharge curve for the same electrolytes.

(c) Battery charge retention for cycles with different values of current insertion.

(d) Energy efficiency for various cycles.
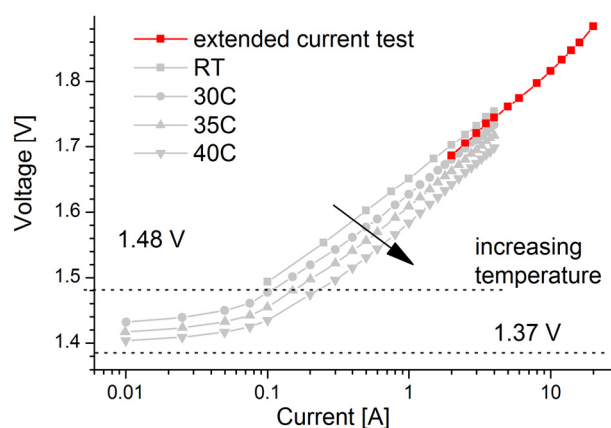
Supplementary Figure 6, Extended battolyser Current-Voltage range.

The potential reached in electrolysis mode versus the applied currents. Experiments without temperature regulation in red, plotted with data from Fig. 6 in gray. At 20A (corresponding to 100mA/cm^2) the electrolysis efficiency is still close to 80% at temperatures well below 40 ^{o}C. For the nominal battery capacity of 10Ah the 20A corresponds to a charge rate of 2C; much higher than would be normally used for daytime charge and night time discharge, but it shows the available operational flexibility.
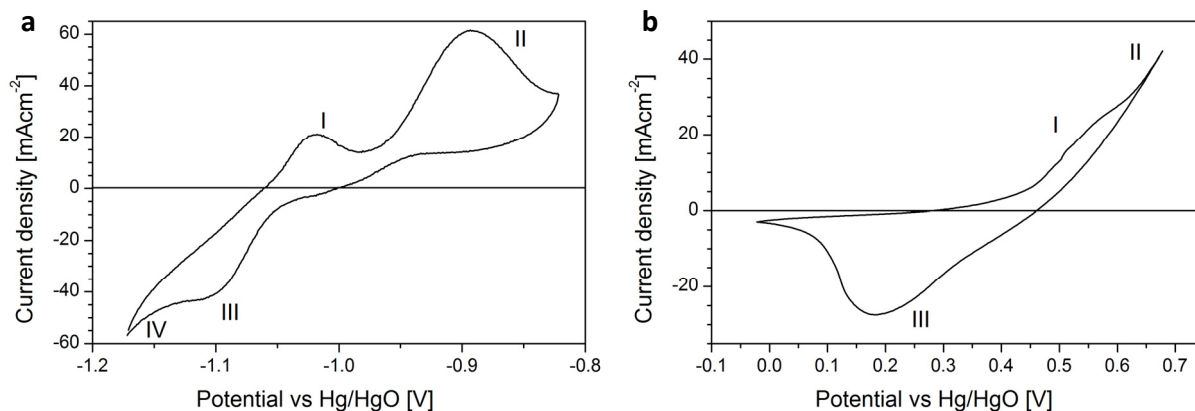
Supplementary Figure 7, Cyclic Voltammograms of the electrodes.

(a) Iron electrode, current density vs. electrode potential (scan rate 1 mV/s, temperature 20˚C). The sweep is restricted to the first discharge plateau of the iron electrode. The redox-couple for the iron electrode ($Fe/Fe(OH)_2$) is indicated by the maximum peak of the anodic cycle II together with peak III of the cathodic cycle. Peak IV represents hydrogen evolution. Peak I of the anodic cycle may be attributed to the formation of initial $Fe(OH)_2$ layers or oxidation of adsorbed hydrogen atoms[4].

(b) Nickel electrode, current density vs. electrode potential (scan rate 0.025 mV/s, temperature 20˚C). The redox-couple for the nickel-electrode ($Ni(OH)_2/NiOOH$) is indicated by peak I in the anodic cycle together with peak III of the cathodic cycle.[5] Peak II in the anodic cycle represents oxygen evolution. At point II $Ni(OH)_2$ has been converted to $NiOOH$, the active oxygen evolution catalyst.
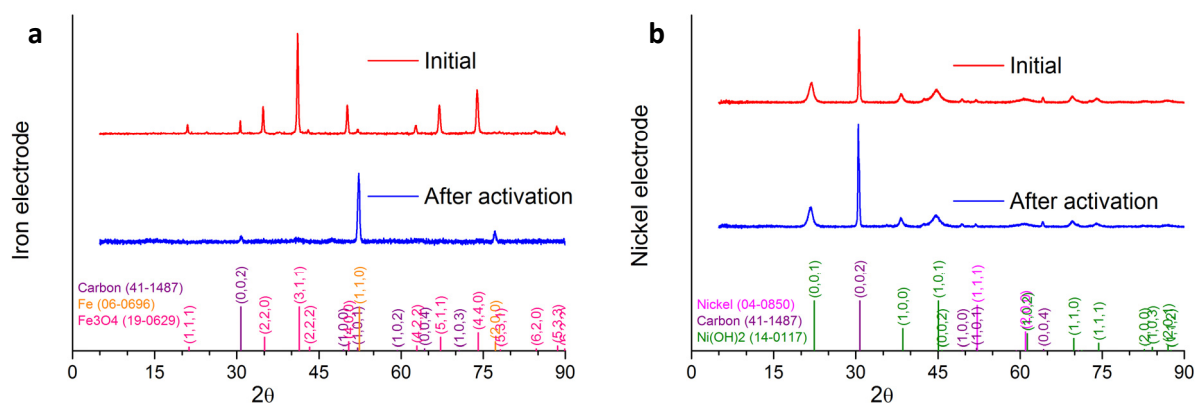
Supplementary Figure 8, XRD-data of initial and cycled electrode materials (X-ray source: Co K_α with wavelength of 1.78897Å, the vertical scale is Counts [a.u.] and the background is removed.)

(a) Initial: Iron electrode material before activation; the diffraction peaks show the as prepared electrode material Fe_3O_4 with a small amount of iron and graphitic carbon. After activation in the cell the metallic Fe formed in the charged state is clearly visible, while Fe_3O_4 has almost completely been reduced.

(b) Initial: β-$Ni(OH)_2$ electrode material before and after activation in the cell. The large line broadening is indicating approximate crystallite sizes of ~ 14nm, that remain constant after cycling. The charged NiOOH is X-ray amorphous as a result of small particle size and lattice plain defects, which has also been reported for the Ni electrode of a nickel-metal hydride battery.[6] The conductive graphitic carbon additive is recognised from the characteristic [002] diffraction peak.

Figure	Charging		Discharging		Electrolysis		Efficiency		
	Capacity [Ah]	Energy [Wh]	Capacity [Ah]	Energy [Wh]	Capacity [Ah]	Energy [Wh]	$\eta_{battery}$ [-]	$\eta_{electrolysis}$ [-]	η_{overal} [-]
5	25.89	42.61	15.86	20.29	10.03	14.85	0.476	0.348	0.825
SF3a black	60.00	101.05	14.94	18.94	45.06	66.69	0.187	0.660	0.847
SF3a red	60.00	99.19	14.77	18.75	45.23	66.95	0.189	0.675	0.864
SF3a blue	60.00	96.41	14.53	18.44	45.47	67.30	0.191	0.698	0.889
SF3b	99.00	165.35	53.50	69.71	45.50	67.35	0.422	0.407	0.829
SF3c	99.00	161.66	53.70*)	71.11	45.30	67.04	0.440	0.415	0.855
SF3d	48.21	80.41	16.27	21.07	31.94	47.27	0.262	0.588	0.850
SF3e	56.29	97.72	19.76	25.99	36.54	54.07	0.266	0.553	0.819

*) see sub-cycle information below

Figure	Temperature [°C]	Charge Rate	Discharge rate	Observed weight loss [g]	Theoretical weight loss due to electrolysis [g]	Observed/ Theoretical Weight loss [-]
SF3a black	30	C/3.33	C/10	15.83	15.14	1.046
SF3a red	30	C/5	C/10	15.81	15.20	1.040
SF3a blue	30	C/10	C/10	15.37	15.28	1.006
SF3b	RT	C/3.33	C/10	15.80	15.29	1.033
SF3c	Variable	Variable*)	Variable*)	**15.65**	**15.22**	**1.028**
SF3d	40C	C/3.33 & C/2.5	C/5	11.52	10.73	1.074
SF3e	RT	C/2.5	C/5	12.58	12.28	1.024

*) see sub-cycle information below

Sub-cycle in Figure SF3c	Rate	Charge Insertion [Ah]	Energy [Wh]	Rate	Discharge Capacity [Ah]	Energy [Wh]
1	C/3.33	9.00	14.46	C/10	4.00	5.35
2	C/4	9.00	14.41	C/20	4.00	5.43
3	C/3.33	9.00	14.73	C/10	4.00	5.37
4	C/4	9.00	14.58	C/20	4.00	5.41
5	C/3.33	9.00	14.85	C/10	4.00	5.35
6	C/4	9.00	14.64	C/20	4.00	5.40
7	C/3.33	9.00	14.87	C/10	4.00	5.34
8	C/4	9.00	14.67	C/20	4.00	5.39
9	C/3.33	9.00	14.90	C/10	4.00	5.33
10	C/4	9.00	14.69	C/20	4.00	5.39
11	C/3.33	9.00	14.86	C/10	13.70	17.35
Sum		99.00	161.66		53.70	71.11

Supplementary Table 1, Cycle capacities, energies, efficiencies and water losses for the cycles in Fig. 5 and Supplementary Fig. (SF) 3a-3e.

The cycle in Supplementary Fig. 3c has one of the highest aggregated current insertion in Fig. 4 and Supplementary Fig. 4 (cycle 113). The cycle from Fig. 5 is number 111. The Electrolysis Energy yield is calculated from Capacity (Ah) * 1.48V (HHV of hydrogen, see Experimental section).
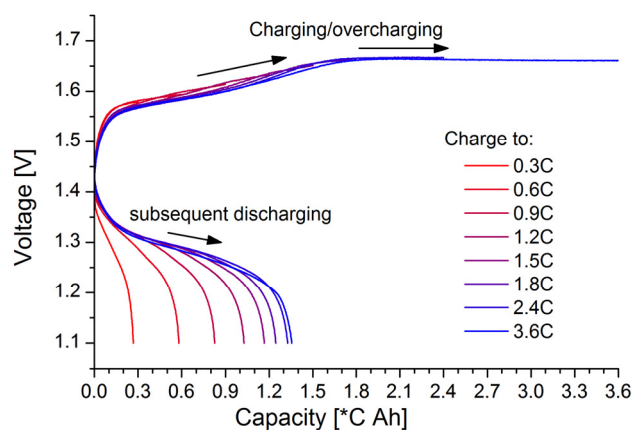
Supplementary Figure 9, Capacity vs Voltage graphs of the same cycles in Fig. 3a.

Charge insertion to the indicated values between 0.3C and 3.6C with subsequent discharge to 1.1V; charge rate C/5; discharge rate C/10; C=10Ah. Test conditions: thermally insulated cell.

Charging		Discharging		Electrolysis		Efficiency		
Capacity [Ah]	Energy [Wh]	Capacity [Ah]	Energy [Wh]	Capacity [Ah]	Energy [Wh]	$\eta_{battery}$ [-]	$\eta_{electrolysis}$ [-]	η_{overal} [-]
3.00	4.70	2.68	3.41	0.32	0.48	0.727	0.102	0.829
6.00	9.49	5.80	7.45	0.20	0.29	0.786	0.031	0.816
9.00	14.31	8.26	10.63	0.73	1.09	0.743	0.076	0.819
12.00	19.19	10.28	13.20	1.72	2.55	0.688	0.133	0.821
15.00	24.10	11.67	14.97	3.33	4.92	0.621	0.204	0.825
18.00	29.11	12.46	15.98	5.54	8.20	0.549	0.282	0.831
24.00	39.10	13.27	17.00	10.73	15.88	0.435	0.406	0.841
36.00	59.11	13.56	17.27	22.44	33.21	0.292	0.562	0.854

Supplementary Table 2, Charge, energy and efficiency data from cycles in Fig. 3a.

Test conditions: thermally insulated cell; charge rate C/5; discharge rate C/10.

Charging		Discharging		Electrolysis		Efficiency		
Capacity [Ah]	Energy [Wh]	Capacity [Ah]	Energy [Wh]	Capacity [Ah]	Energy [Wh]	$\eta_{battery}$ [-]	$\eta_{electrolysis}$ [-]	$\eta_{overall}$ [-]
3.00	4.67	3.10	3.94	-0.10	-0.14	0.843	-0.031	0.812
6.00	9.50	5.81	7.49	0.19	0.28	0.788	0.029	0.818
9.00	14.39	8.11	10.47	0.89	1.31	0.728	0.091	0.819
12.00	19.35	9.98	12.87	2.02	2.99	0.665	0.155	0.820
15.00	24.33	11.30	14.56	3.70	5.47	0.598	0.225	0.823
18.00	29.37	12.03	15.42	5.97	8.83	0.525	0.301	0.826
24.00	39.90	12.96	16.54	11.04	16.34	0.415	0.409	0.824
30.00	50.00	13.63	17.44	16.37	24.23	0.349	0.485	0.833
36.00	59.87	13.88	17.74	22.12	32.74	0.296	0.547	0.843
48.00	80.38	14.55	18.51	33.45	49.50	0.230	0.616	0.846
60.00	101.05	14.94	18.94	45.06	66.69	0.187	0.660	0.847

Supplementary Table 3, Charge, energy and efficiency data for cycles used to make Fig.3b.

Test conditions: regulated temperature of 30˚C; charge rate C/3.33; discharge rate C/10. These cycles are corresponding to cycles 247-258 in Fig. 4 and Supplementary Fig. 4.

References to ESI

1. S. U. Falk and A. J. Salkind, *Alkaline storage batteries*, John Wiley & Sons, 1969.
2. D. Linden and T. B. Reddy, *Handbook of Batteries Third Edition*, McGraw-Hill, 2001.
3. R. Kinzelbach, *Stahlakkumulatoren*, VARTA Batterie AG, Hannover, 1974.
4. M. K. Ravikumar, T. S. Balasubramanian, A. K. Shukla and S. Venugopalan, *Journal of Applied Electrochemistry*, 1996, **26**, 1111-1115.
5. G. A. Snook, N. W. Duffy and A. G. Pandolfo, *Journal of Power Sources*, 2007, **168**, 513-521.
6. J. J. Biendicho, M. Roberts, D. Noreus, U. Lagerqvist, R. I. Smith, G. Svensson, S. T. Norberg, S. G. Eriksson and S. Hull, *J. Mater. Res.*, 2015, **30**, 407-416.